2013 IEEE International Conference on Robotics and Automation (ICRA)
Karlsruhe, Germany, May 6-10, 2013

Squeeze Grasping of Deformable Planar Objects with Segment Contacts and Stick/Slip Transitions

Feng Guo Huan Lin Yan-Bin Jia
Department of Computer Science
Iowa State University
Ames, IA 50011, USA
fguo,linhuan,jia@iastate.edu

Abstract— **Robotic grasping of a deformable object is difficult not simply due to the high computational cost of deformable modeling. More fundamentally, the difficulty lies in a wrench space that changes under deformation, with growing contact areas, and subject to varying slip/stick modes in these areas. This paper presents a grasping strategy by squeezing the object with two fingers. An analysis based on the finite element method (FEM) proves equilibrium and uniqueness of deformation during the action, and leads to a (improved) quadratic time deformation update from the displacements of as few as two contact nodes. An event-driven algorithm is then presented to track the contact regions during a squeeze, and determine the stick/slip mode of every node in contact. The contacts supply the constraints needed for deformation update using FEM. Several experiments with a Barrett Hand have been conducted for validation.**

I. Introduction

Grasping deformable objects is inherently different from grasping rigid ones for which two types of analysis have been developed. Form closure on a rigid object eliminates all of its degrees of freedom, while force closure keeps the object in equilibrium with the ability to resist any arbitrary external wrench. A deformable object has infinite degrees of freedom, which makes form closure impossible. Also, the grasp wrench space changes as the object deforms, which makes force closure analysis inapplicable.

Robot grasping of deformable objects is an under-researched area not only due to the high cost of physics-based deformable modeling, but also for some fundamental mechanics reasons. The initial contact point between a finger and an object grows into an area due to deformation. The points within the contact area may switch mode between slip and stick, making a contact mode analysis necessary to accurately characterize the process. The torques exerted by the fingers vary as the object's geometry and contact modes change, which is different from grasping a rigid body where torques are invariant under specified grasping forces.

Our approach to grasping of deformable objects has been conceived with characteristics to address the above issues. We choose to specify desired displacements of the grasping fingers rather than the forces they exert, for several reasons. First, displacement constraints are usually sufficient for computing the deformation. Second, forces obtained using the FEM automatically ensure equilibrium. Angular momentum is conserved under force equilibrium [2, 49–52]. Third, in practice it is much easier to control a finger's position than the exerted force. Finally, exact force magnitudes are not much of our concern as long as an object can be grasped.

To update the deformed shape, we track the varying set of finger contacts and their modes (stick or slip) and use them as constraints, as grasping continues. This will lead to a contact mode analysis with event detection that is quite different from the one performed on a rigid body.

Computation of a small deformation based on linear elasticity comes down to solving either a system of fourth order differential equations (generally with no closed-form solution), or practically, a large linear system using FEM. The latter approach takes sub-cubic time in the number of discretization nodes, which is typically high for accurate modeling. A large deformation, meanwhile, can only be modeled by nonlinear elasticity (and computed using the even more expensive nonlinear FEM).

To make things worse, repeated deformation computations are needed for verifying a grasp, finding a successful one, or choosing one with the best quality. The standard FEM procedure always exerts fixed node constraints by eliminating the corresponding rows and columns from the object's stiffness matrix. In grasping, whenever the fingers are relocated, the (reduced) stiffness matrix varies. An improvement is only possible if computation works directly on the original stiffness matrix, as is to be presented in this work.

A. Assumptions and Paper Outline

We make several assumptions about the grasping task. The object is isotropic, and either planar or thin 2-$\frac{1}{2}$D. Gravity is ignored. Two grasping fingers are in the same plane, and make frictional area contacts with the object. The grasp yields small deformations to which the linear elasticity theory is applicable. Deformation happens instantaneously such that no dynamics is considered. In this paper, we picture deformation as a continuous process happening in an infinitesimal amount of time.

This paper investigates two-finger grasping of an object by squeezing it. The action is equivalent to keeping one finger still, while translating the other finger toward it. We call this a *squeeze grasp*. The segment connecting the two initial contact points must lie inside their friction cones to ensure

978-1-4673-5642-8/13/$31.00 ©2013 IEEE

deformation. Under the squeeze, each contact point will grow into a region.

Section II will briefly review some basic results from linear elasticity and FEM. Section III will describe how to compute the deformation of an object given the displacements of several boundary points. Section IV will present an event-driven algorithm to compute a grasp. Several experiments will be described in Section V, and some discussion on future research will follow in Section VI.

B. Related Work

Rigid body grasping is an extensively studied area rich with theoretical analysis, algorithmic syntheses, and implementations with robotic hands [1]. In particular, two-finger force-closure grasps of 2-D objects are well understood and efficiently computable for polygons [10] and piecewise-smooth curved shapes [11].

Much less work exists on grasping of deformable objects. In [14], a model for deformable contact regions under a grasp was introduced to predict contact forces without concern of grasp computation or modeling of global deformation. Simulation accuracy and efficiency could be improved based on derived geometric properties at deformable contact [9]. The work [15] investigated deformable modeling of shell-like objects that have already been grasped.

Bounded force-closure was proposed in [16]. Visual and tactile information was effective on controlling the motion of a grasped deformable object [7]. The deformation-space (D-space) approach [6] characterized the optimal grasp of a deformable part as one where the potential energy needed to release the part equals the amount needed to squeeze it to its elastic limit — hence the object could not escape.

In [5], an iterative FEM-based solution was given for 2D elastic contact problems with no friction. It was extended to deal with friction in [13] with iterative updating of the contact zone and the modes of individual nodes within the zone: stick, slip, contact break or establishment. This event-based approach was extended in [3] to handle geometric and physical nonlinearities as well as node-edge contacts, solving for the exact loading condition from prescribed displacements. The load rather than displacement was specified.

Our recent work [8] considered squeeze grasps under specified forces. Unrealistic constraints had to be imposed at the contacts for modeling shape deformation. The grasp synthesis algorithm was also too inefficient to be applicable to solid 2-D objects.

II. Finite Element Method

This section reviews planar linear elasticity, describing all displacement fields representing rigid body transformations, and characterizing the null space of the stiffness matrix of an unconstrained object. The result will be used in design of a squeeze-based grasping strategy.

Consider a solid object bounded by a generalized cylinder parallel to the z-axis, and two planes $z = 0$ and $z = h > 0$, where h is small compared to the generalized cylinder's dimensions in the xy-plane. We consider *plane stress* parallel to the xy-plane, which assumes zero normal stress σ_z and shear stresses τ_{xz} and τ_{yz} in the x-z and y-z planes. Under a displacement field $(u(x,y), v(x,y))^T$, every point $(x,y)^T$ inside the object displaces to $(x+u, y+v)^T$. The normal strains are $\epsilon_x = \frac{\partial u}{\partial x}$ and $\epsilon_y = \frac{\partial v}{\partial y}$, and the shear strain is $\gamma_{xy} = \frac{\partial u}{\partial y} + \frac{\partial v}{\partial x}$. The strain energy is [4, p. 302]:

$$U = \frac{hE}{2(1+\nu)} \iint_S \left(\frac{\epsilon_x^2 + 2\nu\epsilon_x\epsilon_y + \epsilon_y^2}{1-\nu} + \frac{\gamma_{xy}^2}{2} \right) dxdy, \quad (1)$$

where $E > 0$ and $-1 \le \nu \le \frac{1}{2}$ are Young's modulus and Poisson's ratio of the material, respectively.

Theorem 1: Under linear elasticity, any displacement field $(u(x,y), v(x,y))^T$ that yields zero strain energy is linearly spanned by $(1,0)^T$, $(0,1)^T$, and $(-y,x)^T$.

It is a known result. The fields $(1,0)^T$ and $(0,1)^T$ describe rigid body translations along the x and y axes respectively, and $(-y,x)^T$ approximates small rotations about the origin.

Generally without closed form of the strain energy integral (1), it is computed using the FEM. The object's cross section is discretized into a finite number of triangular elements with vertices (or nodes) $\boldsymbol{p}_k = (x_k, y_k)^T$, for $1 \le k \le n$. We place the origin at the centroid of these vertices so $\sum_{k=1}^n \boldsymbol{p}_k = 0$. The first m vertices, $m \le n$, lie on the boundary in counterclockwise order.

Under deformation, each node $\boldsymbol{p}_k$ is displaced by $\boldsymbol{\delta}_k = (\delta_{kx}, \delta_{ky})^T$. The displacement field of an element is linearly interpolated by its vertices' displacements. Assembling the strain energies of all elements gives the total strain energy $U = \frac{1}{2}\boldsymbol{\Delta}^T K \boldsymbol{\Delta}$, where K is the $2n \times 2n$ *stiffness matrix*. Note that K is both symmetric (by Betti's law [12, pp. 447–448]) and positive semi-definite (since U is non-negative).

That U is zero if and only if $K\boldsymbol{\Delta} = 0$ implies $\boldsymbol{\Delta} \in \mathrm{null}(K)$, the null space of K. Under Theorem 1, we see that $\mathrm{null}(K)$ is spanned by $\boldsymbol{w}_x = (1,0,\ldots,1,0)^T$, $\boldsymbol{w}_y = (0,1,\ldots,0,1)^T$, and $\boldsymbol{w}_r = (-y_1, x_1, \ldots, -y_n, x_n)^T$.

Thus, $\mathrm{rank}(K) = 2n-3$. Let λ_i and $\boldsymbol{v}_i$, $i = 1, \cdots 2n-3$, be the positive eigenvalues and corresponding eigenvectors. The null eigenvectors $\boldsymbol{v}_{2n-2}, \boldsymbol{v}_{2n-1}$ and $\boldsymbol{v}_{2n}$ are normalized $\boldsymbol{w}_x, \boldsymbol{w}_y, \boldsymbol{w}_r$ respectively. We have the Spectrum Decomposition $K = V\Lambda V^T$, where $V = (\boldsymbol{v}_1, \ldots, \boldsymbol{v}_{2n})$ and $\Lambda = \mathrm{diag}(\lambda_1, \ldots, \lambda_{2n-3}, 0, 0, 0)$.

Aggregate the applied forces at all nodes into vector $\boldsymbol{F}$. Note that $\boldsymbol{F}$ is non-zero only at some boundary nodes. Minimization of the total potential energy $U - \boldsymbol{F}^T\boldsymbol{\Delta}$ yields $K\boldsymbol{\Delta} = \boldsymbol{F}$. Since K is singular, constraints will have to be imposed by the fingers to prevent any rigid body movement.

III. Deformation from Specified Displacements

Denote by $\boldsymbol{p}_{i_1}, \ldots, \boldsymbol{p}_{i_s}$ the positions of some boundary nodes. Suppose the displacement of $\boldsymbol{p}_{i_j}$ is given as $\boldsymbol{\delta}_{i_j} = \boldsymbol{d}_j$ and $\boldsymbol{f}_k = 0, \forall k \ne i_1, \ldots, i_s$. We would like to determine the forces $\boldsymbol{f}_{i_j}$ exerted at all $\boldsymbol{p}_{i_j}$'s, and the displacements of all n nodes. Note that the displacements of $s > 1$ nodes must be specified, otherwise the object is underconstraint and a rigid body movement is resulted.

A. Deformation

Substitute the spectral decomposition $K = V\Lambda V^T$ into $K\boldsymbol{\Delta} = \boldsymbol{F}$, we obtain $\Lambda V^T\boldsymbol{\Delta} = V^T\boldsymbol{F}$. Expansion of the above yields $\boldsymbol{v}_k^T\boldsymbol{\Delta} = \frac{1}{\lambda_k}\boldsymbol{v}_k^T\boldsymbol{F}$, $k = 1, \ldots, 2n-3$. With them we decompose $\boldsymbol{\Delta}$ in terms of $\boldsymbol{v}_1, \boldsymbol{v}_2, \ldots, \boldsymbol{v}_{2n}$:

$$\boldsymbol{\Delta} = \sum_{k=1}^{2n-3} \frac{1}{\lambda_k}(\boldsymbol{v}_k^T\boldsymbol{F})\boldsymbol{v}_k + \sum_{k=2n-2}^{2n} g_k\boldsymbol{v}_k, \tag{2}$$

where $g_k = \boldsymbol{v}_k^T\boldsymbol{\Delta}$, $k = 2n-2, 2n-1, 2n$.

Write $\bar{\boldsymbol{v}}_k = (v_{2i_1-1,k}, v_{2i_1,k}, \ldots, v_{2i_s,k})^T$, for $1 \le k \le 2n$, $\boldsymbol{f} = (\boldsymbol{f}_{i1}^T, \ldots, \boldsymbol{f}_{is}^T)^T$, and $\boldsymbol{g} = (g_{2n-2}, g_{2n-1}, g_{2n})^T$. Since $\bar{\boldsymbol{v}}_k^T\boldsymbol{f} = \boldsymbol{v}_k^T\boldsymbol{F}$, from (2) we have, for $l = 1, \ldots, n$,

$$\boldsymbol{\delta}_l = \sum_{k=1}^{2n-3} \frac{1}{\lambda_k}\begin{pmatrix} v_{2l-1,k} \\ v_{2l,k} \end{pmatrix}\bar{\boldsymbol{v}}_k^T\boldsymbol{f} + \begin{pmatrix} \frac{1}{\sqrt{n}} & 0 & -\frac{y_l}{\rho} \\ 0 & \frac{1}{\sqrt{n}} & \frac{x_l}{\rho} \end{pmatrix}\boldsymbol{g}, \tag{3}$$

Substitute $\boldsymbol{d}_j$ for $\boldsymbol{\delta}_{i_j}$ in (3), for $1 \le j \le s$, and assemble the resulting equations in the form: $A\boldsymbol{f} + B\boldsymbol{g} = \boldsymbol{d}$, where $A = \sum_{k=1}^{2n-3}\frac{1}{\lambda_k}\bar{\boldsymbol{v}}_k\bar{\boldsymbol{v}}_k^T$, $B = (\bar{\boldsymbol{v}}_{2n-2}, \bar{\boldsymbol{v}}_{2n-1}, \bar{\boldsymbol{v}}_{2n})$, and $\boldsymbol{d} = (\boldsymbol{d}_1^T, \ldots, \boldsymbol{d}_s^T)^T$. Note that A is symmetric. Meanwhile, left multiplications of $\boldsymbol{v}_{2n-2}^T, \boldsymbol{v}_{2n-1}^T, \boldsymbol{v}_{2n}^T$ respectively with $K\boldsymbol{\Delta} = \boldsymbol{F}$ yield $B^T\boldsymbol{f} = 0$, which implies force equilibrium $\sum_{j=1}^s \boldsymbol{f}_{i_j} = 0$ and torque equilibrium $\sum_{j=1}^s \boldsymbol{p}_{i_j} \times \boldsymbol{f}_{i_j} = 0$. Combine $B^T\boldsymbol{f} = 0$ with $A\boldsymbol{f} + B\boldsymbol{g} = \boldsymbol{d}$:

$$M\begin{pmatrix} \boldsymbol{f} \\ \boldsymbol{g} \end{pmatrix} = (\boldsymbol{d}^T, 0, 0, 0)^T. \tag{4}$$

where $M = \begin{pmatrix} A & B \\ B^T & 0 \end{pmatrix}$. Note that M is also symmetric.

B. Uniqueness of Deformation

Now we will establish that the matrix M is nonsingular so $(\boldsymbol{f}, \boldsymbol{g})^T$ can be uniquely determined from (4) given $\boldsymbol{d}$.

Lemma 2: For $s \ge 2, \boldsymbol{x} \ne 0$, $\boldsymbol{x}^T A\boldsymbol{x} > 0$ if $B^T\boldsymbol{x} = 0$.

Proof: Consider the matrix $\bar{V} = (\bar{\boldsymbol{v}}_1, \ldots, \bar{\boldsymbol{v}}_{2n})$. Since these selected rows from V are orthogonal to each other, $\mathrm{rank}(\bar{V}) = 2s$, which is also the matrix's column rank. Therefore, the vector $\boldsymbol{x}$ of dimension $2s$ must be spanned by the columns of $\bar{V}$.

Suppose $B^T\boldsymbol{x} = 0$. Because $s \ge 2$, $\mathrm{rank}(\bar{V}) \ge 4$ and $\mathrm{rank}(B^T) \le 3 < \mathrm{rank}(\bar{V})$. We infer that the vector $\boldsymbol{x}$, orthogonal to $\bar{\boldsymbol{v}}_{2n-2}, \bar{\boldsymbol{v}}_{2n-1}, \bar{\boldsymbol{v}}_{2n}$, is a linear combination of $\bar{\boldsymbol{v}}_1, \bar{\boldsymbol{v}}_2, \ldots, \bar{\boldsymbol{v}}_{2n-3}$. There exists some $\bar{\boldsymbol{v}}_j$, $1 \le j \le 2n-3$ such that $\bar{\boldsymbol{v}}_j^T\boldsymbol{x} \ne 0$. Therefore, $\boldsymbol{x}^T A\boldsymbol{x} = \boldsymbol{x}^T\left(\sum_{k=1}^{2n-3}\frac{1}{\lambda_k}\bar{\boldsymbol{v}}_k\bar{\boldsymbol{v}}_k^T\right)\boldsymbol{x} \ge \frac{1}{\lambda_j}(\bar{\boldsymbol{v}}_j^T\boldsymbol{x})^2 > 0$. ■

Theorem 3: The matrix M is nonsingular for $s \ge 2$.

Proof: We prove that $M\binom{\boldsymbol{f}}{\boldsymbol{g}} \ne 0$ whenever $\boldsymbol{f} \ne 0$ or $\boldsymbol{g} \ne 0$. There are two cases:

- $B^T\boldsymbol{f} \ne 0$. $\begin{pmatrix} A & B \\ B^T & 0 \end{pmatrix}\binom{\boldsymbol{f}}{\boldsymbol{g}} = \binom{A\boldsymbol{f}+B\boldsymbol{g}}{B^T\boldsymbol{f}} \ne 0$.
- $B^T\boldsymbol{f} = 0$. We have

$$\begin{aligned} & (\boldsymbol{f}^T, \boldsymbol{g}^T)\begin{pmatrix} A & B \\ B^T & 0 \end{pmatrix}\begin{pmatrix} \boldsymbol{f} \\ \boldsymbol{g} \end{pmatrix} \\ = \; & \boldsymbol{f}^T A\boldsymbol{f} + \boldsymbol{g}^T B^T\boldsymbol{f} + \boldsymbol{f}^T B\boldsymbol{g} \\ = \; & \boldsymbol{f}^T A\boldsymbol{f} > 0 \qquad (B^T\boldsymbol{f} = 0, \text{ and Lemma 2}). \end{aligned}$$

This implies $M(\boldsymbol{f}, \boldsymbol{g})^T \ne 0$. ■

Corollary 4: If $\boldsymbol{d}$ is part of a rigid body displacement, then $\boldsymbol{f} = 0$.

Proof: In case $s = 1$, we know that $\mathrm{rank}(B^T) = 2$, so $B^T\boldsymbol{f} = 0$ implies $\boldsymbol{f} = 0$.

In case $s \ge 2$, $(\boldsymbol{f}, \boldsymbol{g})^T = M^{-1}(\boldsymbol{d}^T, 0, 0, 0)^T$. Let $c_i = \boldsymbol{d}^T\boldsymbol{v}_{2n-3+i}/||\boldsymbol{v}_{2n-3+i}||$, for $i = 1, 2, 3$, and $\boldsymbol{\delta} = (\boldsymbol{v}_{2n-2}, \boldsymbol{v}_{2n-1}, \boldsymbol{v}_{2n})(c_1, c_2, c_3)^T$. Then $\boldsymbol{\delta}$ is a rigid body displacement and it contains $\boldsymbol{d}$. So $F = K\boldsymbol{\delta} = 0$. The uniqueness of solution indicates that $\boldsymbol{f}$ is the corresponding part of F, and is thus 0. ■

C. Running Time

Since M is nonsingular, we solve $(\boldsymbol{f}, \boldsymbol{g})^T$ from (4). Then each δ_l is computed from (3) in $O(n)$ time, taking the small number of contacts as a constant. Thus the total computation takes $O(n^2)$ time after SVD which takes $O(n^3)$ time.

IV. Two-Finger Squeeze Grasp

We place two fingers $\mathcal{F}_1$ and $\mathcal{F}_2$, with identical semicircular tips of radius r and centers $\boldsymbol{o}_1$ and $\boldsymbol{o}_2$, on the object at boundary nodal points $\boldsymbol{p}_i$ and $\boldsymbol{p}_j$, respectively. The finger orientations are irrelevant assuming that only the tips will be in contact. Also, $\boldsymbol{o}_1$ and $\boldsymbol{o}_2$ must lie on the object's normal at $\boldsymbol{p}_i$ and $\boldsymbol{p}_j$. The finger placement is thus fully specified.

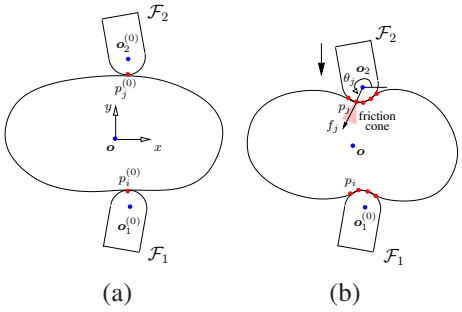

Fig. 1. Object (a) before and (b) after a squeeze grasp.

As shown in Fig. 1(a), we place the origin at the center of the object, and let the y-axis point toward $\boldsymbol{p}_j$. Finger $\mathcal{F}_1$ is motionless, while finger $\mathcal{F}_2$ translates in the direction $\boldsymbol{p}_i - \boldsymbol{p}_j$ by a distance $d > 0$, which is referred to as the *squeeze depth.* As the squeeze continues, some boundary nodal points may come into contact with the fingers, as illustrated in Fig. 1(b), while others may break contact with them. A node in contact may be sticking to a fingertip or sliding on it. The *contact configuration* at the squeeze depth d describes which nodal points are in contact, and among them, which are sticking or sliding. The contact configuration is critical because it yields position and force constraints that are needed by FEM to compute the deformed shape under the squeeze. We will incrementally track the contact configuration as d increases.

A. Contact Configuration

The squeeze depth will be sequenced into $d_0 = 0 < d_1 < \cdots$, such that at $d = d_l$ some event happens to trigger a change in the contact configuration. For $d > d_l$, we use the

new configuration and evaluate the changes in $\boldsymbol{f}$ and $\boldsymbol{\Delta}$ using the FEM, and predict d_{l+1}.

At d_l, we maintain two sets: T of nodes sticking with a finger, and P of nodes sliding on a finger. Translate $\mathcal{F}_2$ down by a small extra distance $\epsilon > 0$. Suppose T and P do not change as d varies within $[d_l, d_l + \epsilon)$.

For each node $\boldsymbol{p}_k \in T \cup P$, denote by θ_k its polar angle with respect to the center of the contact fingertip. See Fig. 1(b) for an illustration on $\boldsymbol{p}_j$. Denote $\boldsymbol{\delta}_k = \boldsymbol{\delta}_k^{(l)}$ and $\theta_k = \theta_k^{(l)}$ when $d = d_l$. We can determine the displacement $\boldsymbol{\delta}_k = \boldsymbol{\delta}_k^{(l)} + \mathring{\boldsymbol{\delta}}_k$ when $d = d_l + \epsilon$ as follows. If $\boldsymbol{p}_k$ is on $\mathcal{F}_2$,

$$\mathring{\boldsymbol{\delta}}_k = -\epsilon\hat{\boldsymbol{y}} + r \begin{pmatrix} \cos\theta_k - \cos\theta_k^{(l)} \\ \sin\theta_k - \sin\theta_k^{(l)} \end{pmatrix}, \tag{5}$$

where $\hat{\boldsymbol{y}} = \binom{0}{1}$. If $\boldsymbol{p}_k$ is on $\mathcal{F}_1$, the term $-\epsilon\hat{\boldsymbol{y}}$ in (5) vanishes.

A sticking contact at $\boldsymbol{p}_k$ imposes a position constraint $\theta_k = \theta_k^{(l)}$ on deformation. If $\boldsymbol{p}_k$ slips, the contact force $\boldsymbol{f}_k = \boldsymbol{f}_k^{(l)} + \mathring{\boldsymbol{f}}_k$ must stay on one edge of the friction cone at $\boldsymbol{p}_k$ as the node moves. Let $\phi = \tan^{-1}\mu$, where μ is the coefficient of contact friction. This imposes a force constraint:

$$\left(\boldsymbol{f}_k^{(l)} + \mathring{\boldsymbol{f}}_k\right) \times \begin{pmatrix} \cos(\theta_k \pm \phi) \\ \sin(\theta_k \pm \phi) \end{pmatrix} = 0, \tag{6}$$

where the sign '$+$' or '$-$' can be determined either from the previous step or using hypothesis-and-test.

Since equation (4) is linear, we gather the changes $\mathring{\boldsymbol{\delta}}_k$ in the displacements of all contacts into a vector $\mathring{\boldsymbol{d}}$ and replace $\boldsymbol{d}$ with $\mathring{\boldsymbol{d}}$, $\boldsymbol{f}$ with $\mathring{\boldsymbol{f}}$, $\boldsymbol{g}$ with $\mathring{\boldsymbol{g}}$ in (4). Solve for $\mathring{\boldsymbol{f}}$ and $\mathring{\boldsymbol{g}}$. Then in (3), which is also linear, replace $\boldsymbol{f}, \boldsymbol{g}, \boldsymbol{\delta}_l$ with $\mathring{\boldsymbol{f}}$, $\mathring{\boldsymbol{g}}$, $\mathring{\boldsymbol{\delta}}_l$, respectively. This gives us $\mathring{\boldsymbol{\delta}}_l$ and thus $\boldsymbol{\delta}_l$, for $1 \le l \le n$, which are linear in terms of ϵ, $\cos\theta_t$, and $\sin\theta_t$, $\forall \boldsymbol{p}_t \in P$.

Substitute the expression for $\mathring{\boldsymbol{f}}_k$ in (6). This yields an equation linear in ϵ and quadratic in $\cos\theta_t$ and $\sin\theta_t$, for every $\boldsymbol{p}_t \in P$. There are a total of $|P|$ such equations that form a system S in the same number of variables θ_t. Given a value of ϵ, we can solve for these θ_ts. Since ϵ is small, Newton's method converges fast with the initial values $\theta_t^{(l)}$. Hence $\boldsymbol{\Delta}$ and $\boldsymbol{f}$ are updated.

With θ_k known for every sliding contact $\boldsymbol{p}_k$, we can also determine the derivative $\frac{d\theta_k}{d\epsilon}$, which will be used for checking whether a node $\boldsymbol{p}_k$ switches from slip to stick. Differentiate both sides of every equation in the system S with respect to ϵ. This yields a new linear system of $|P|$ equations in $|P|$ derivatives $\frac{d\theta_t}{d\epsilon}$, $p_t \in P$. Simply solve the system.

B. Contact Event Detection

Now we look at how to predict the value of ϵ such that the next event occurs at squeeze distance $d^{(l+1)} = d^{(l)} + \epsilon$ to trigger a change in one or both of the contact sets T and P. There are four types of events described as follows.

1) Event A — New Contact: A boundary node $\boldsymbol{p}_k$ comes into contact with one of the two fingers. This happens when its distance to the center of the contacting fingertip reduces to r, or equivalently, when the following condition holds (assuming the moving finger $\mathcal{F}_2$ to be in contact):

$$||\tilde{\boldsymbol{p}}_k - \tilde{\boldsymbol{o}}_2 + \begin{pmatrix} 0 \\ \epsilon \end{pmatrix}|| = r. \tag{7}$$

Here we denote $\tilde{\boldsymbol{q}}$ as the displaced position of a point $\boldsymbol{q}$. For completeness, we ought to check every boundary node that is currently not in contact with any finger. Often a new contact node is adjacent to an outermost contact node.

To determine the mode of contact for $\boldsymbol{p}_k$, we first hypothesize that it sticks, apply a small extra squeeze, and check if the resulting contact force $\boldsymbol{f}_k$ stays inside the friction cone. If not, the node slips. Add $\boldsymbol{p}_k$ to T or P accordingly.

2) Event B — Contact Break: As ϵ increases, the force $\boldsymbol{f}_k$ at a node $\boldsymbol{p}_k$ varies inside or on one edge of the contact friction cone. When its magnitude reduces to zero, it is about to point into the finger. This implies that the contact breaks when $\|\boldsymbol{f}_k\| = 0$. Remove $\boldsymbol{p}_k$ from P or T that contains it.

3) Event C — Stick to Slip: When the contact force $\boldsymbol{f}_k$ applied on a sticking node $\boldsymbol{p}_k$ is rotating out of the inward friction cone (cf. Fig. 1(b)) as d increases, the contact starts to slip. The rotation of the force $\boldsymbol{f}_k$ at the moment is indicated by its derivative with respect to ϵ. We need to check the conditions:

$$\boldsymbol{f}_k \times \begin{pmatrix} \cos(\theta_k \mp \phi) \\ \sin(\theta_k \mp \phi) \end{pmatrix} = 0 \ \text{ and } \ \mp\frac{d\boldsymbol{f}_k}{d\epsilon} \times \begin{pmatrix} \cos(\theta_k \mp \phi) \\ \sin(\theta_k \mp \phi) \end{pmatrix} > 0 \tag{8}$$

for reaching the left (sign '$-$') or right ('$+$') edge, respectively. Remove $\boldsymbol{p}_k$ from T and add it to P.

4) Event D — Slip to Stick: As ϵ increases, the contact node $\boldsymbol{p}_k$ slides, and its polar angle θ_k with respect to the corresponding fingertip's center varies. Slip changes to stick when $d\theta_k/d\epsilon = 0$. In this case, move $\boldsymbol{p}_k$ from P to T.

C. The Squeeze Algorithm

The algorithm starts at $d = 0$. At step l, it hypothesizes each of the four events for every possible node, and computes the extra squeeze distance ϵ for the first hypothesized event to happen. Let $d_{l+1} = d_l + \epsilon$. Event testing involves solving for ϵ and polar angles θ_t of all sliding contacts $\boldsymbol{p}_t$ from the event condition and the corresponding $|P|$ equations. Analytical solution is difficult if not impossible.

Here we employ a numerical routine that increments the squeeze depth d by a small step size h. Because h is small, Newton's method converges fast in computing θ_t for $\boldsymbol{p}_t \in P$. Checking whether an event happens becomes testing either an inequality or whether an expression changes sign. If no event happens for the current increment h, the algorithm simply continues.

The algorithm terminates if the grasp succeeds when the specified d is reached, or if the grasp fails when all contacts with some finger slip before d is reached.

D. Finger Kinematics

In reality, the robotic fingers may have to rotate while squeezing. Let the changes in orientation of $\mathcal{F}_1$ and $\mathcal{F}_2$ be $\alpha_1(d)$ and $\alpha_2(d)$, respectively, according to hand kinematics. Some of the above derivations need adaption. Redefine θ_k as $\boldsymbol{p}_k$'s polar angle with respect to the center of the fingertip in the finger's local frame. In Equations (5) and (6), and the conditions for Event C and D, θ_k should be replaced by $\theta_k + \alpha_i$ if $\boldsymbol{p}_k$ is on $\mathcal{F}_i$.

V. EXPERIMENTS

We performed experiments using a Barrett Hand on two types of objects: ring-like ones and solid ones. The Barrett Hand was mounted with small spherical finger tips for ringlike objects, and cylindrical tips for solid ones.

A. Ring-like Objects

Two hollow objects displayed in the first column of Fig. 2 were grasped. They were trimmed from cookie cutters. Such an object may be viewed as one swept out by a rectangular cross section with width w and height h along a closed 2-D curve $\boldsymbol{\gamma}(s)$ parametrized by arc length s and having perimeter L. The curve has a displacement field $\boldsymbol{\delta}(s) = \boldsymbol{\alpha}(s)\boldsymbol{t}+\beta(s)\boldsymbol{n}$, where $\boldsymbol{t}$ and $\boldsymbol{n}$ are the unit tangent and normal on the curve. Let κ be its curvature. The strain energy takes the form $U_c = \frac{1}{2}Ew\int_0^L(h\epsilon^2 + \frac{h^3}{12}\zeta^2)ds$ [8], where $\epsilon = \frac{d\alpha}{ds} - \kappa\beta$ is the extensional strain and $\zeta = -\frac{d^2\beta}{ds^2} - \frac{d\kappa}{ds}\alpha - \kappa\frac{d\alpha}{ds}$ is the change in curvature. The curve is discretized into FEM elements with the strain energy U_c written in the form $U = \frac{1}{2}\Delta^T K\Delta$.

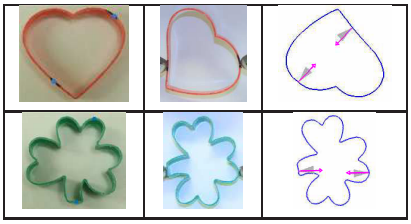

Fig. 2. Successful grasps of two deformable objects.

The two fingers make small area contact with the object that can be approximated by point contact. The analysis from Section III and the squeeze grasp algorithm from Section IV-C carry over. Since each finger has only one contact point, the grasp fails at a squeeze depth when the contact force reaches one edge of the friction cone and slip starts.

Fig. 2 shows two successful grasps in column 2 that agreed with the algorithm's predictions in column 3. The heart-shaped band has physical parameter values $(E, \mu, h, \rho) = (2\text{GPa}, 0.26, 5\text{mm}, 10\%)$, where h is the thickness, and ρ is the *relative* squeeze depth to the distance between the two initial finger contacts. The leaf-shaped band has physical parameter values $(2, 0.26, 5, 11\%)$.

Under a squeeze, the two contact friction cones sometimes rotate toward each other, making the applied forces more aligned with the axes of the cones, and the grasp more stable (Fig. 3(b)). In some other cases, the two cones rotate away from each other, breaking the grasp, as shown in Fig. 3(c).

B. Solid Objects

A 0.1m by 0.1m square made of rubber foam (thickness 0.0254m) was grasped by the Barrett Hand. Fig. 4 compares the actual grasp configuration with one simulated by the squeeze grasp algorithm. In the center, the deformed mesh from simulation is superposed onto the real shape with an almost perfect alignment (average error is 1.3mm while the edge length is 0.1m) after data matching that aims at minimizing discrepancies introduced by the choices of

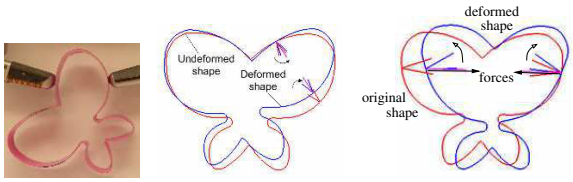

(a) (b) (c)

Fig. 3. During a grasp (a), contact friction cones rotate toward each other (b). During another grasp, they rotate away to break a grasp (c).

coordinate systems in simulation and experiments. Left and right columns compare contact regions by simulation and from experiment, on the two fingers respectively.

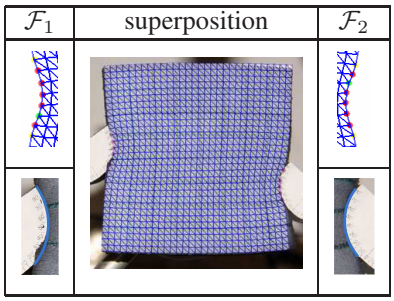

Fig. 4. Grasp configuration with contact regions: simulation vs. experiment.

The contact forces evolve as the squeeze deepens, as shown in Fig. 5. The magnitude of the contact force at each nodal point calculated from simulation was transformed to the force density over curve length, while the direction was represented as its polar angle. The nodal values were then interpolated with cubic splines. The density in the center of the contact is generally bigger than that on the edge. Also, The force on each segment, and the total force, increases with deeper squeeze. The directions of the contact forces show a general trend of decreasing along curve length. As the squeeze continues, the curve spans over more nodes, indicating a growing contact area.

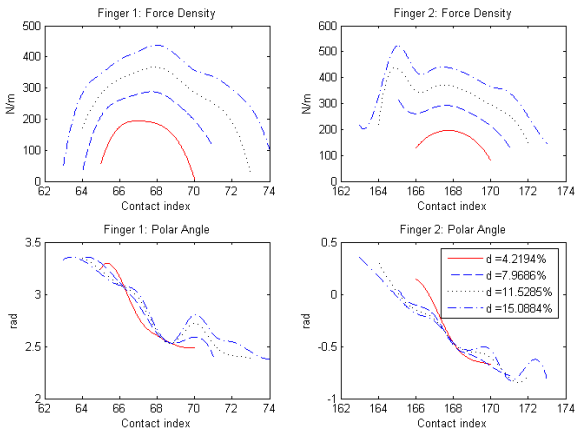

Fig. 5. Force profile. At different relative squeeze depth d, the forces exerted by finger 1 (left column) and 2 (right column) were decomposed to force density (upper row) and polar angle (lower row).

The position of a point in contact with the finger tip can be described by its polar angle with respect to the finger center. Fig. 6 shows movements of sliding contacts as the

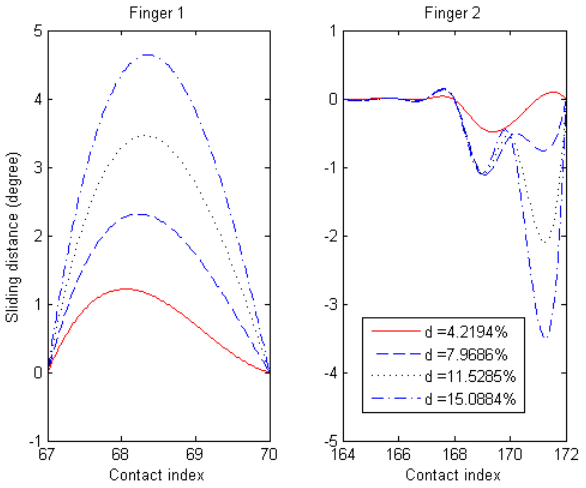

Fig. 6. Sliding profile. Here, d is the relative squeeze depth.

squeeze depth increases. At a squeeze distance, the contact node positions are interpolated by a cubic spline to give a continuous illustration of point movement over the contact segment. As d increases, we can see that the sliding distance of the contacts increases.

C. Sliding/Sticking Transition

Among the four types of events introduced in Section IV, Event A is easy to picture with common sense. Event B was so rare that it was not observed in our experiment. Event C was widely observed in both simulation and experiment wherever friction is insufficient. Fig. 7 shows some grasps in which Event C happened. Each of the yellow and red arrows in the middle and lower rows emphasizes one point on the objects and fingertips respectively. Note the changes in their relative positions when squeeze deepened, indicating an Event C. Event D happened a lot less than Event C. Fig. 8

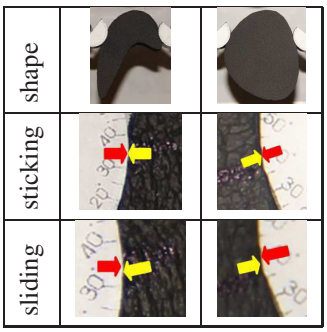

Fig. 7. Event C

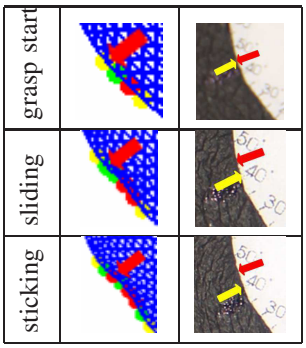

Fig. 8. Event D

shows a point on the object in three configurations: initial stick (first row), intermediate slip (second row), and final stick again(third row).

VI. Discussion and Future Work

This paper studies grasping planar deformable objects by squeezing them with two fingers. One key idea is to specify displacements rather than forces, and use them as constraints to the object. Another one is to keep track of and predict the contact configuration at a squeeze depth (needed for computing the deformation) in an event-driven manner. We have conducted several experiments to validate the squeeze grasp algorithm, rotation of a contact friction cone, growth in a contact region, and pointwise contact mode switch.

In the next phase, we would like to design a quality measure for grasps and investigate grasp optimization.

VII. Acknowledgment

Support for this research was provided in part by Iowa State University, and in part by the National Science Foundation through the grant IIS-0915876. Any opinions, findings, and conclusions or recommendations expressed in this material are those of the author(s) and do not necessarily reflect the views of the National Science Foundation. Thanks to ISU undergraduate Trenton Anagnostopoulos for writing the mesh generation code.

References

[1] A. Bicchi and V. Kumar, "Robotic grasping and contact: a review," in *Proc. IEEE Intl. Conf. Robot. Autom.*, 2000, pp. 348–353.

[2] A. F. Bower, *Applied Mechanics of Solids*, CRC Press, Boca Raton, Florida, 2009.

[3] N. Chandrasekaran, W. E. Haisler, and R. E. Goforth, "A finite element solution method for contact problems with friction", *Int. J. Num. Meth. Engr.*, vol. 24, pp. 477-495, 1987.

[4] S. H. Crandall, N. C. Dahl and T. J. Lardner, An Introduction to the Mechanics of Solids, 2nd edition, McGraw-Hill, 1978.

[5] A. Francavilla and O. C. Zienkiewicz, "A note on numerical computation of elastic contact problems," *Int. J. Num. Meth. Engr.*, vol. 9, pp. 913–924, 1975.

[6] K. Gopalakrishnan and K. Goldberg, "D-space and deform closure grasps of deformable parts," *Int. J. Robot. Res.*, vol. 24, pp. 899–910, 2005.

[7] S. Hirai, T. Tsuboi, and T. Wada, "Robust grasping manipulation of deformable objects," in *Proc. IEEE Symp. Assembly and Task Planning*, 2001, pp. 411-416.

[8] Y.-B. Jia, F. Guo, and T. Jiang, "On two-finger grasping of deformable planar objects," in *Proc. IEEE Int. Conf. Robot. Autom.*, 2011, pp. 5261–5266.

[9] Q. Luo and J. Xiao, "Geometric properties of contacts involving a deformable object," in *Proc. IEEE Symp. Haptic Interfaces Virtual Env. Tele. Sys.*, 2006, pp. 533–538.

[10] V. D. Nguyen, "Constructing force-closure grasps," *Int. J. Robot. Res.*, vol. 7, pp. 3–16, 1988.

[11] J. Ponce, D. Stam, and B. Faverjon, "On computing two-finger force-closure grasps of curved 2D objects," *Int. J. Robot. Res.*, vol. 12, pp. 263–273, 1993.

[12] A. S. Saada, *Elasticity: Theory and Applications*, Kreiger Publishing Co., Malabar, Florida, 1993.

[13] T. D. Sachdeva and C. V. Ramakrishnan. "A finite element solution for the two-dimensional elastic contact problems with friction," *Int. J. Num. Meth. Engr.*, vol. 17, pp. 1257-1271, 1981.

[14] P. R. Sinha, J. M. Abel, "A contact stress model for multifingered grasps of rough objects," *IEEE Trans. on Robot. Automat.*, vol. 8, pp. 7–22, 1992.

[15] J. Tian and Y.-B. Jia, "Modeling deformable general parametric shells grasped by a robot hand," *IEEE Trans. on Robot.*, vol. 26, pp. 837–852, 2010.

[16] H. Wakamatsu, S. Hirai and K. Iwata, "Static analysis of deformable object grasping based on bounded force closure," in *Proc. IEEE/RSJ Intl. Conf. Intell. Robots and Systems*, 1996, pp. 3324-3329.